# UNIVERSITY *of York*

# Novel Starbon/HACS-supported *N*-heterocyclic carbene-iron(III) catalyst for efficient conversion of fructose to HMF

Avtar S. Matharu*[a], Duncan J. Macquarrie[a], Suleiman Ahmed[a], Badriya Almonthery[a], Yoon-Sik Lee[b] and Yohan Kim[b].

[a]Green Chemistry Centre of Excellence, Department of Chemistry, University of York, UK. YO10 5DD.
[b]School of Chemical and Biological Engineering, Seoul National University, 1 Kwanak-Ro, Kwanak-Gu, Seoul 151-742, Republic of Korea.

**ABSTRACT:** Iron-nitrogen heterocyclic carbenes (Fe-NHCs) have come to the fore because of their ability to be employed in diverse catalytic applications ranging from C-C cross-coupling and C-X bond formation to substitution, reduction, polymerization, and dehydration. The detailed synthesis, characterisation and application of novel heterogeneous Fe-NHC catalysts immobilised on mesoporous expanded starch and Starbon™ 350 for facile fructose to HMF conversion is reported. Both catalyst types showed good performance for the dehydration of fructose to HMF when the reaction was explored at 100 ∘C and varying time (10 min, 20 min, 0.5 h, 1 h, 3 h and 6 h): Fe-NHC S350, highest HMF yield, 81.7 % (t=0.5 h), TOF=169 h$^{-1}$, fructose conversion of 95 % and HMF selectivity of 85.7 %, and; Fe-NHC expanded HACS, highest yield, 86 % (t=0.5 h), TOF=206 h$^{-1}$, fructose conversion of 87 % and HMF selectivity of 99 %. An iron-loading of 0.26 and 0.30 mmol/g was achieved for the Fe-NHC expanded starch and Fe-NHC Starbon™ 350, respectively.

## Introduction

Iron-nitrogen heterocyclic carbenes (Fe-NHC's) have come to the fore because of their ability to be employed in diverse catalytic applications ranging from cross coupling and C-X bond formation to substitution, reduction, polymerization, dehydration and recently their unusual application as promising photosensitizers.[1,2] NHCs are special among other carbenes because they are stable, directly synthesized, can attach to metals with different oxidation states and can form organometallic complexes that are stable as catalysts. [3], [4] Moreover, iron is abundant, of low toxicity and benign, widely recycled and, thus, conforms to elemental sustainability. The chemical transformation of biomass to platform molecules can be extremely challenging due to complex chemistries and/or is tediously slow. Fe-NHC's have been used for fructose to HMF conversions, affording good yields. However, most of the systems are homogeneous and therefore present challenges in product separation and or catalyst recovery and recycling.

On the other hand, functional porous materials have been used in catalysis providing many opportunities. [5] Mesoporous solids present advantages with respect to conventional porous solids when they are used as catalyst supports, due to their high surface area, large pore size and thermal and hydrothermal stabilities.[5-8] Our approach combined the catalytic advantages of Fe-NHC's and the large surface area, pore size and stability of mesoporous supports producing a perfect catalyst for heterogeneous catalysis. Carbon catalysts and carbon supported catalysts can facilitate a variety of reactions for the catalytic conversion of biomass into chemicals. [9] The Green Chemistry Centre of Excellence has developed a range of biobased mesoporous carbonaceous materials derived from waste polysaccharides termed Starbon™, possessing large surface areas ranging from 150 up to 500 m² g$^{-1}$ obtained via controlled pyrolysis of expanded polysaccharide precursors (expanded starch). [10] The large surface area and mesoporous nature of Starbon™ makes it an important and efficient support for heterogeneous catalysis. [11]

As summarised in Figure 1, herein, the first synthesis of a novel iron-nitrogen heterocyclic carbene (Fe-NHC) supported on expanded starch (**1a**) and Starbon™ 350 (**1b**) as potential catalysts for the dehydration of fructose (**2**) to 5-(hydroxymethyl) furfural (HMF) (**3**) is reported. Expanded high amylose corn starch (**4**) was used as a support, and precursor for Starbon™-350, because it is (bio)renewable, and readily available from a variety of waste biomass types. HMF (**3**) is considered a renewable material and an excellent platform molecule because it can be acquired from biomass through chemical dehydration using homogeneous and/or heterogeneous acid catalysts. [12,13] The presence of both hydroxymethyl (-CH$_2$OH) and aldehyde (-CHO) moieties within HMF makes it a reactive molecule affording further downstream products. HMF is a precursor for: 2,5-dimethylfuran (DMF), a biofuel and which itself leads to levulinic acid; 2,5-diformylfuran (DFF);5-hydroxy-4-keto-2-pentenoicacid; 2,5-furan dicarboxylic acid (FDA), and; 2,5-dihydroxymethylfuran. [14]

The dehydration of various carbohydrate precursors to 5-HMF in an acidic biphasic system under microwave heating was reported by Delbecq *et al*. [15] More recently the conversion of carbohydrate to HMF using hydrothermally stable Nb-SBA-15 catalysts in a biphasic system has been reported by Peng *et al*. showing good yield of HMF (61.8%). [16] Another investigation on fructose to HMF conversion was by Garcés *et al*. in which they investigate the aqueous phase conversion of hexoses into HMF and levulinic acid in the presence of hydrochloric acid. [17]
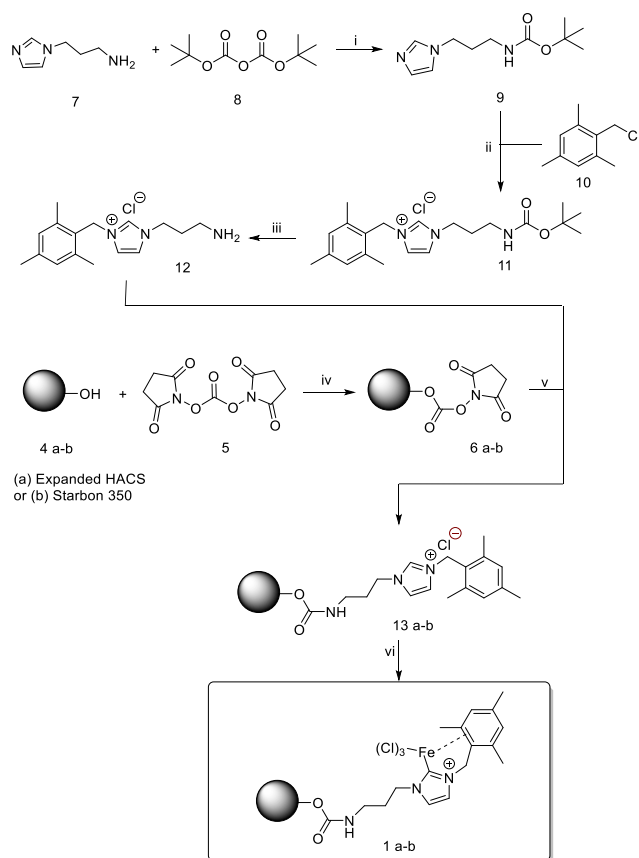
Reagents and conditions: i. NaHCO$_3$, CPME, 4 h, rt; ii. CPME, 80 °C,18 h; iii. TFA, CPME, 50 oC, 6 h; iv. DMAP, propylene carbonate, 80 °C,18 h; v. TEA, propylene carbonate, 80 °C,18 h; vi. KtOBu, FeCl$_3$, propylene carbonate, 80 °C, 18 h

**Figure 1. Synthetic route to iron-NHC catalysts 1a and 1b.**

## Results and Discussion

The desired Fe-NHC catalyst (eg. **1a-b**) was successfully acquired from the reaction between (**13**), in the presence of potassium-*tert*-butoxide as base and propylene carbonate as solvent, and iron(III) chloride in good yield (61.5%).

Expanded HACS (**4a**) or Starbon™-350 (**4b**) suspended in propylene carbonate was successfully converted in to succinimidyl carbonate derivative (**6**), in the presence of *N,N*-disuccinimidyl carbonate (**5**) and catalyzed by DMAP, in good yield (60%). In certain cases, this conversion has been carried in dimethyl formamide (DMF),[18] a toxic dipolar aprotic solvent, which is removed by washing with copious amounts of water post reaction resulting in considerable amounts of aqueous waste. The latter is usually incinerated but because DMF is a nitrogen containing solvent, NOx emissions are produced. On the other hand, propylene carbonate (used in this case, see Figure 1) is a green(er) alternative produced from (waste) carbon dioxide and propylene oxide. Unlike DMF, incineration of propylene carbonate affords carbon dioxide and water only.

The theoretical degree of substitution (DS) of starch (**4a**) is 3 because it comprises three hydroxyl moieties per each anhydroglucose unit, i.e., at C2, C3 and C6. As the stoichiometry of starch (**4**) with respect to *N,N*-disuccinimidyl carbonate (**5**) is 1:3, initially the conversion to its succinimidyl carbonate derivative (**6**) was

performed using a slight excess of (**5**), i.e., 3.16 molar equivalents or 0.16 molar excess, to afford a succinimidyl carbonate degree of substitution (DS) of 0.33±0.11 corresponding to 20.92±4.88% of succinimidyl carbonate activation on the expanded HACS. The low DS may be due to inaccessibility of the hydroxyl moieties within starch despite using expanded HACS (**4a**) and due to steric hindrance associated with the bulky succinimdyl carbonate group. It is envisaged that substitution has most likely taken place preferentially on the C6-OH because it is least hindered.

### Characterization of Fe-NHC bio-based catalyst (1a-b)
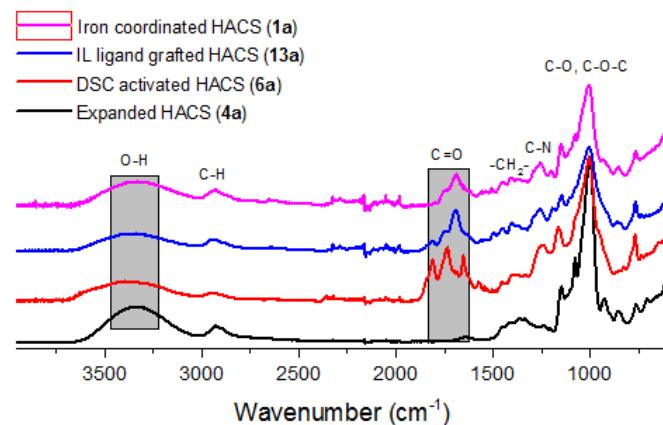
**FT-IR**



Figure 1. FT-IR spectra for expanded HACS (**4a**), succinimidyl carbonate activated HACS (**6a**), ligand grafted DSC activated HACS (**13a**) and Fe-NHC catalyst (**1a**).
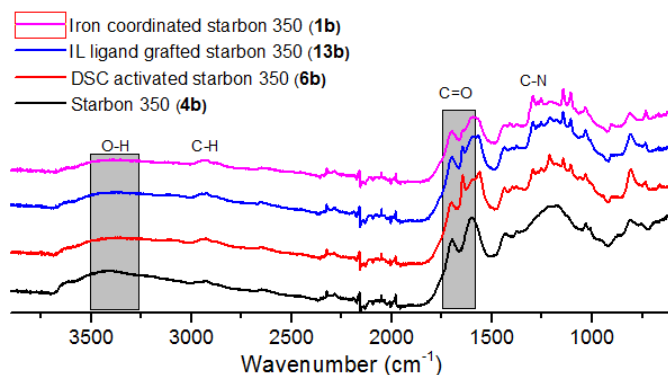


Figure 2.FT-IR spectra for S350 (**4b**), succinimidyl carbonate activated S350 (**6b**), ligand grafted S350 (**13b**) and Fe-NHC S350 (catalyst) (**1b**).

The FT-IR spectra of expanded HACS (**4a**) and its corresponding surface modified forms are depicted in Figure 2. Several absorbance bands arising from starch in the region 1000-1200 cm$^{-1}$, corresponding to C-O, C-C, C-O-H bond stretching and C-O-H bending,[19] are evident along with a broad band centred at 3341 cm$^{-1}$ associated with O-H stretching synonymous with hydroxyl groups in expanded HACS (**4a**).[20] The spectra of DSC-modified HACS (**6a**) showed new absorbance bands at 1813, 1738, 1653 cm$^{-1}$ assigned to carbonyl (C=O str), and 1239 cm$^{-1}$ assigned to imide (C-N) vibration corresponding to newly attached carbonyl groups on HACS surface. The absorbance band patterns of IL based ligand grafted HACS (**13a**) showed newly

grafted imidazolium (1257, 1192 cm$^{-1}$) and formed carbonyl (C=O) in carbamate group (1695 cm$^{-1}$).

For Starbon™-350 (figure 3), shows C=C at 1600 cm$^{-1}$ and one carbonyl stretching band 1702 cm$^{-1}$. However, in the DSC activated Starbon™-350 (6b), two additional bands appear at 1566 cm$^{-1}$ and 1678 cm$^{-1}$ assigned to carbonyl of the DSC group attached during activation. This argument is also supported by a decrease in the intensity of the OH stretching at 3353 cm$^{-1}$ from Starbon™-350 (4b) to the DSC activated Starbon™-350 (6b), signifying that many OH groups on the Starbon™-350 were activated by the succinimidyl carbonate group.

Moreover, the IR spectra of the ligand grafted Starbon™-350 (13b) indicates a disappearance of a band at 1567 cm$^{-1}$ and a corresponding decrease of the band at 1647 cm$^{-1}$ assigned to the C=O stretching of the carbamate. This however, indicates that the ligand is successfully grafted on the DSC group as proposed in the reaction equation. This argument is further supported by complementary $^{13}$C CP MAS NMR data shown in Figure 4.
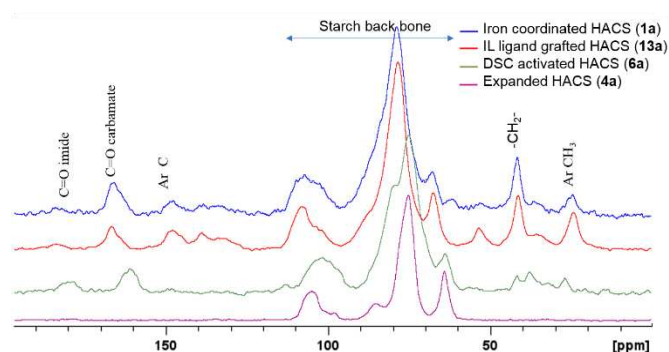
### 13C CPMAS NMR



Figure 3.. $^{13}$C CPMAS NMR spectra for expanded HACS (4a), succinimidyl carbonate activated HACS (6a), ligand grafted activated HACS (13a) and Fe-NHC catalyst (1a)
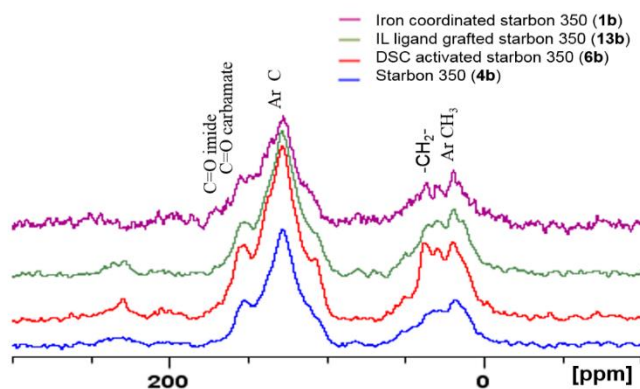


Figure 4.$^{13}$C CPMAS NMR spectra for Starbon 350 (4b), succinimidyl carbonate activated S350 (6b), ligand grafted activated S350 (13b) and Fe-NHC catalyst (1b)

NMR signals observed at 61.8, 82.1 and 101 ppm were assigned to C-6, C-4 and C-1 in expanded HACS (4a), respectively. [21,22] The major signal at 72.5 ppm is assigned to C-2, -3, -5. With expanded HACS activation process (see spectra for DCS activated HACS, 6a), DSC (N,N-disuccinimidyl carbonate) groups were attached to hydroxyl groups on HACS surface and caused some signal shifts on the starch backbone. Carbonyl signal from succinimidyl carbonate group appeared in 162, and 180 ppm.

However, on the starch support, C-1 was affected by the succinimidyl carbonate groups and shifted from 106 ppm to 102 ppm. After ligand (12) binding to afford 13a , the carbonyl signal at 180 ppm assigned to the imide of the succinimidyl group almost disappears leaving the signal at 166 ppm assigned to the carbamate which also shifted from 162 ppm due to ligand binding. On the starch support C-2, -3, -5 shifted from 75.5 ppm to 79.4 ppm, with C6 also shifted from 61.8 ppm to 66.2 ppm due to ligand binding.

The successful ligand binding was further confirmed by the appearance of new signals at 23, 40-51, 127-137 ppm and 142 ppm corresponding to aromatic CH$_3$, imidazole -CH$_2$-, carbons of imidazole ring and aromatic carbon of the attached imidazole ligand respectively. [23-25] The IL grafted HACS (13a) has one carbonyl group connected with HACS and ligand. Similarly, the $^{13}$C CPMAS spectra of IL grafted HACS (13a) also shows one carbonyl peak at 160 ppm. Moreover, due to iron coordination reaction, peaks of iron coordinated starch were slightly shifted, except the resonance in 51 ppm corresponding to next carbon of imidazole group.

The $^{13}$C CPMAS spectra of Starbon™ 350 and its modified forms (see Figure 5) show similar resonance changes as described for the HACS materials. However, the ligand grafted Starbon™ 350 (13b) shows new signals at 23, 40-51, assigned to aromatic CH$_3$, imidazole -CH$_2$-, and carbons of imidazole ring, respectively.

It was difficult to assign all the aromatic carbons, and most importantly the carbonyls of the imide and carbamate group of the DSC were masked within the signals for Starbon™ itself.

### Thermogravimetry

STA was used to examine the thermal decomposition of expanded HACS (4a) and its modified compounds (6a), (13a) and (1a) as shown in Figure 6. The thermal decomposition of expanded starch (4a) was as per literature [245-333 °C] [26]; Initial loss of moisture (approx. 9% water) both physi- and chemisorbed from 25 °C to 135°C is observed followed by main degradation and decomposition (T$_d$, 326 °C) of glycosidic bonds and the carbohydrate skeleton from 300-350 °C corresponding to approximately 70% mass loss. Heating from 400-600 °C afforded a further, smaller, mass loss (~5%). Approximately, 18% of residue remained at the end of the analysis. The thermal decomposition of the subsequent compounds, i.e., succinimidyl carbonate starch (6a) and ligand grafted starch (13a) showed a similar decomposition profile to expanded starch (4a). Both show an initial mass (approx. 5%) from 25-135 °C again due to bound water within starch but a small and gradual mass loss is observed from 135-200 °C, which may be due to residual propylene carbonate solvent. Interestingly, conversion of (4a) to (6a), lowers the decomposition temperature from 326 °C (4a) to 321 °C (6a) indicating that the structure and packing within starch has been disrupted. In particular, the extensive inter- and intra-hydrogen bonding network associated with the hydroxyl groups of starch is disrupted as modification (DS, 0.33±0.11%) reduces the number of hydroxyl groups. Evidence for substitution may also be considered by the fact that approx. 24% of residue is left at the end of decomposition (600 °C) of (6a) compared with approx. 18% residual mass for (4a). The extra mass is from the additional elemental contribution (mainly carbon) from succinimidyl carbonate moiety. Similarly, the greatest residual mass is observed for decomposition of (13a) which has the greatest proportion of carbon with respect to compounds (4a) and (6a), which also has the lowest decomposition temperature (T$_d$, 300 °C) due to greatest structural and chemical modification.

Figure 7. TG (top) and DTG (bottom) for Starbon 350 (**4b**), succinimidyl carbonate activated Starbon 350 (**6b**), ligand grafted Starbon 350 (**13b**) and Starbon 350 Fe-NHC catalyst (**1b**).

Similarly, the thermograms for the equivalent Starbon™ 350 tethered materials are shown in Figure 7. An early mass loss was observed at approximately 40 °C to 120 °C due to loss of both physio and chemisorbed water in each of the Starbon™ materials. The unmodified Starbon™-350 (**4b**) was fairly stable from 150 to 310 °C after which a major weight loss temperature (550 °C), corresponding to the breakdown of the Starbon™ backbone is reached. However, in the modified Starbon™ sample (**6b**) the major weight loss temperature is decreased by the chemical modification; 528 °C for succinimidyl carbonate activated Starbon™-350 (**6b**), 506 °C for imidazolium ligand grafted Starbon™-350 (**13b**), and 528 °C for Fe coordinated Starbon™ 350 (**1b**). This indicates that the functionality attached on the Starbon™ surface affects the intermolecular interaction and hence decreases the decomposition temperature. However, an increase in the residual mass of about 2.41% (a characteristic reddish-brown residue) was obtained in the Fe coordinated Starbon™ 350. This entails that Fe is contained in the sample.
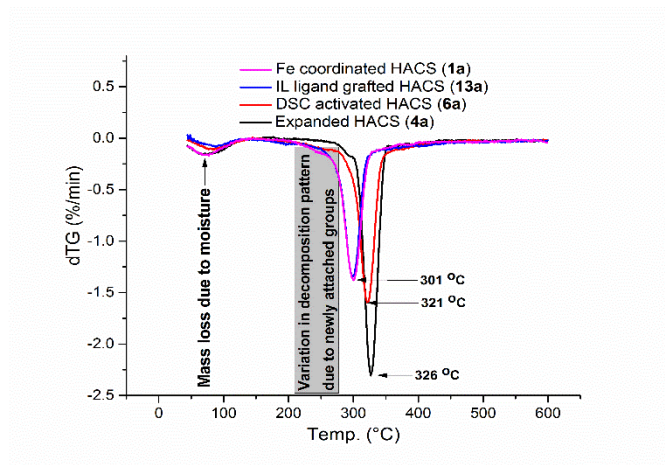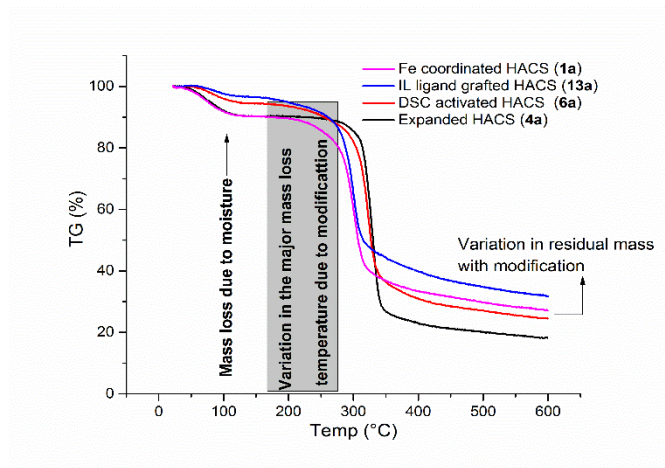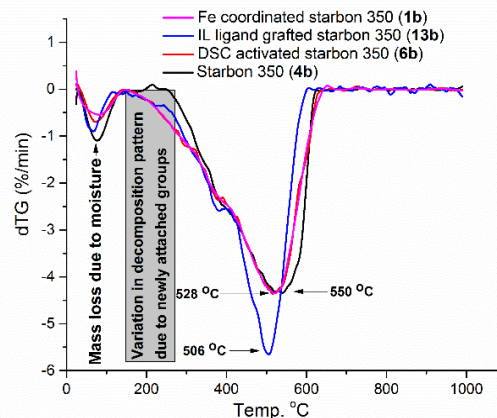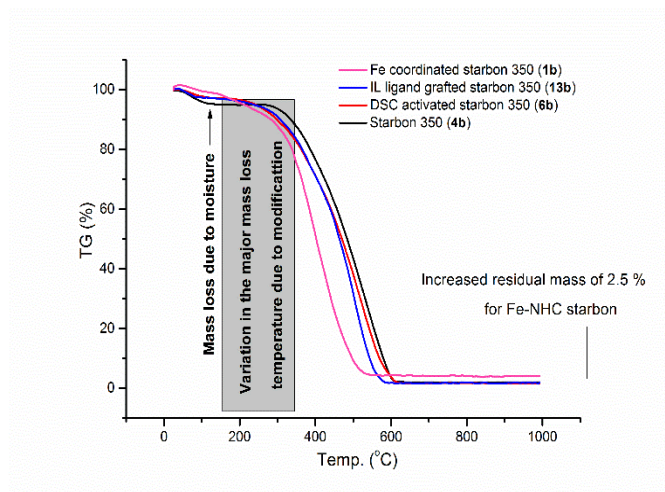


Figure 6. TG (top) and dTG (bottom) for expanded HACS (**4a**), succinimidyl carbonate activated HACS (**6a**), ligand grafted DSC activated HACS (**13a**) and Fe-NHC catalyst (**1a**).

The thermogram for the Fe-NHC catalyst (**1a**) shows slight enhancement in thermal stability ($T_d$, 301 °C) with respect to its precursor ((**13a**), $T_d$ 300 °C) which may be related to additional energy associate with iron-carbene complexation, *i.e.,* Fe-NHC. Interestingly, slightly less residual mass was observed at 600 °C for (**1a**) than for (**13a**) probably due to iron itself triggering or catalyzing decomposition of starch. However, this is to be further investigated.



#### CHN and ICP-MS Elemental analysis

The succinimidyl carbonate and NHC ligand loadings were determined from nitrogen content measurement by CHN elemental analysis. The Fe loading on the other hand was determined from ICP-MS elemental analysis. Table 1 below give a summary of the loadings in mmol/g of support material.

Table 1. Loading levels (mmol/g) of succinimidyl carbonate, NHC ligand and Fe on expanded HACS and Starbon 350.

| Support | Loading level (mmol/g) | | |
|---|---|---|---|
| | Succinimidyl carbonate | NHC ligand | Fe |
| Expanded HACS | 2.09 | 1.23 | 0.26 |
| Starbon 350 | 1.18 | 0.63 | 0.31 |

## Mössbauer Spectroscopy



Fe-NHC expanded HACS (1a)
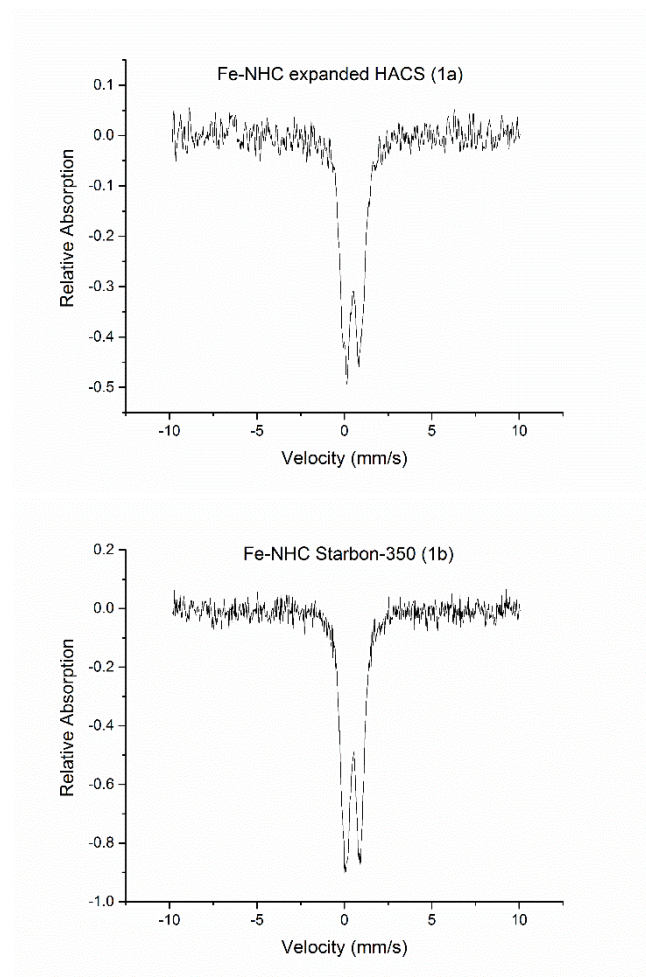


Fe-NHC Starbon-350 (1b)

Figure 8. Mössbauer spectrum of Fe-NHC expanded HACS (Top, **1a**) and Fe-NHC Starbon 350 (Bottom, **1b**).

The Mössbauer spectra for expanded HACS (**1a**, Figure 8 top) and S350 fabricated catalysts (**1b**, Figure 8 bottom), respectively, confirms the presence of iron in the form of $Fe^{3+}$. A characteristic isomer shift of 0.47 coupled with quad. splitting of 0.81 are representative of $Fe^{3+}$.[27] The presence of iron, as well as oxygen and nitrogen, was further evidenced by XPS analyses.

.

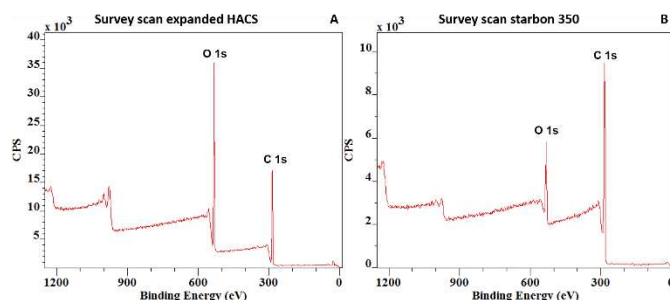## X-Ray Photoelectron spectroscopy

### Survey Scan



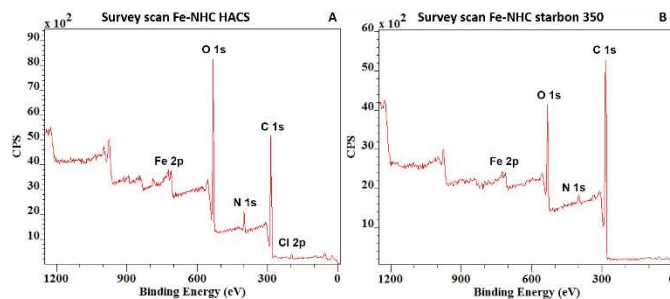Figure 9. XPS survey data of (A) Expanded HACS (**4a**) (B) Starbon 350 (**4b**).



Figure 10. XPS survey data of (A) Fe-NHC HACS catalyst (**1a**) (B) Fe-NHC starbon 350 catalyst (**1b**).

The XPS survey spectrum of expanded HACS (**4**), (figure 9 A) and Starbon™ 350 (figure 9 B), have two main absorption bands typically at 283.45 and 530.87 eV corresponding to C1s and O1s energy levels, respectively. However, the Fe-NHC expanded HACS catalyst (**1a**) (figure 10 A) and Fe-NHC Starbon™ 350 catalysts (**1b**) (figure 10 B) has four absorption peaks at about 283.45, 399.88, 533.78 and 711.34 eV corresponding to C1s, N1s, O1s and Fe2p, respectively, providing clear evidence for the presence of iron and nitrogen in addition to the expected carbon and oxygen already in the unmodified supports

### Carbon 1s peak

Comparing the fitted carbon 1s XPS spectra of the unmodified expanded HACS (**4a**) and S350 (**4b**) supports to that of Fe-NHC modified expanded HACS (**1a**) and S350 (**1b**) (Fig. S1-S2 of ESI), additional carbon peaks at 283.6, 286.1 and 289.2 assigned to C-C(Ar), C-N and C=O are observed. [28] These additional peaks are believed to come from compound (**12**) attached on the expanded HACS.

### Oxygen 1s peak

The fitted O1s spectra (Fig. S3-S4 of ESI), the expanded HACS (**4a**) shows two peaks at 531.5 and 533.5eV assigned to C-O and O-H bonds in the expanded HACS. However, the XPS peak of the Fe-NHC expanded HACS (**1a**) shows additional peak at 533 eV corresponding to C=O.[29] Another important and striking difference is the decrease in the O-H peak intensity which confirms the loss of some hydroxyl groups from the expanded HACS (**4a**) due to activation. This decrease in the intensity of the hydroxyl peak in the expanded HACS and the corresponding appearance of a new C=O peak in the Fe-NHC expanded HACS, indicates and further prove the successful attachment of (**12**) on the expanded HACS surface leading to the formation of (**1a**).

The O1s spectra of the starbon 350 (**4b**), figure 17, shows three peaks at 529.5, 531.5 and 534.2 eV assigned to C=O, C-O and O-H bonds in the starbon 350 respectively. [29] However, the deconvolution of the XPS peak of the Fe-NHC starbon 350 (**1b**) shows another important and striking difference with the decrease in the O-H peak intensity which confirms the loss of some

hydroxyl groups from the starbon 350 support (**4b**). This decrease in the intensity of the hydroxyl peak and the corresponding increase of the C=O peak in the Fe-NHC starbon 350, indicates and further prove the successful attachment of **12** on the starbon 350 support (**4b).**

### Nitrogen 1s peak

The appearance of a nitrogen 1s peak at 400eV in the XPS survey spectra of the Fe-NHC expanded HACS (**1a**) and Fe-NHC Starbon™ 350 (**1b**) which was originally absent in the survey spectrum of the unmodified expanded HACS (**4a**) and Starbon™ 350 (**4b**) supports, is a clear indication that a new compound containing nitrogen has been attached to the expanded HACS and Starbon™ 350 supports. Further deconvolution of the N1s peak (Fig. S5-S6 of ESI) indicates three different nitrogen bonding environments at 398.3, 399.2 and 401.3eV assigned to N-H, C-N, and C=N respectively. This however, is believed to have come from compound **12** attached to the supports.

### Iron 2p peaks

The appearance of a Fe doublet peak with the Fe $2p_{1/2}$ at 711eV in the spectra of the Fe-NHC expanded HACS (**1a**) and Fe-NHC Starbon™ 350 (**1b**) (Fig. S5-S6 of ESI) confirms the presence of iron predominantly in the +3 oxidation state. [30-32]

### Nitrogen Porosimetry and SEM

The BET surface area, pore width and pore volume of expanded HACS (**4a**) and its subsequent Fe-NHC modified form, (**1a**) were determined using nitrogen adsorption porosimetry (see Table 1. in ESI). On modification of expanded HACS (**4a**) through to the desired Fe-NHC (**1a**) the BET surface area decreased: 186.7 $m^2/g$ (**4a**); and; 135.5 $m^2/g$ (**1a**). The subsequent decrease in surface area and pore volume may be explained by possible blocking and filling of the porous structure both by the ligand and importantly iron. The pore size distribution shows a broad peak within the mesoporous region (2-50 nm). [33] The BET surface area of Starbon™ 350 also shows a corresponding decrease with modification, 332 $m^2/g$ (**4b**) to 138 $m^2/g$ (**1b**). These data prove that activation of the expanded HACS, grafting of the ligand and coordination of iron maintains porosity with significant retention of mesopores.

To further investigate changes in surface structure (topography) and porosity, SEM (figure 11) was performed on expanded HACS (**4a**), ligand immobilized HACS (**13a**) and Fe-NHC catalyst (**1a**). Although, the images reveal limited information it can be seen that the extent of pitting and mesh-like network (surrogate for porosity) decreases on the surface from (**4a**) to (**1a**) which may also be related to the corresponding decrease in BET surface area discussed earlier. Similarly, figure 12 indicates that Starbon™ 350 support (**4b**) also contains a network of pores and that the porosity is retained during modification process.
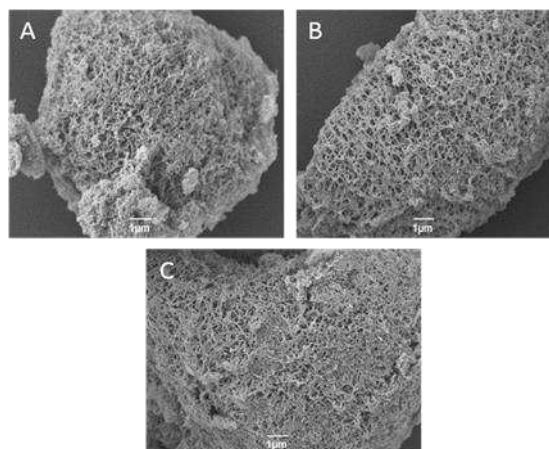


Figure 11. SEM micrographs of (A) expanded HACS (**4a**) (B) Ligand grafted expanded HACS (**13a**) and (C) Fe-NHC expanded HACS (**1a**).
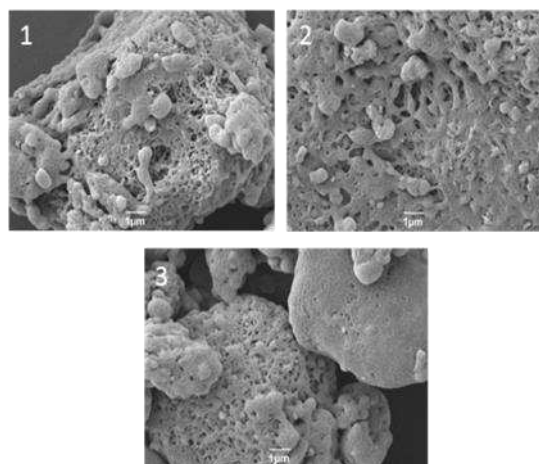


Figure 12. SEM micrographs of (1) Starbon 350 (**4b**), (2) Ligand grafted Starbon 350 (**13b**) and (3) Fe-NHC Starbon 350 (**1b**).

### Catalytic activity: Fructose (2) to HMF (3) conversion

Initially, a series of control experiments were undertaken in the absence of fructose (**2**), *i.e.*, DMSO-$d_6$ and Fe-NHC catalyst (**1**), in order to confirm the carbohydrate (starch) support was itself not acting as a sacrificial or competing substrate with respect to fructose and to investigate iron leaching. However, no significant change was observed. The filtrate was analysed by ICP-MS to reveal negligible trace of iron in solution (79.49 ppb) which may be due to surface trapping of residual iron(III) chloride and/or iron oxide. Nevertheless, it can be assumed that the Fe-NHC catalyst (**1a**) is neither being sacrificed nor does it leach any complexed iron.

In addition, an *insitu* NMR study was conducted to investigate influence of temperature which revealed temperature dependency for fructose to HMF conversion. No significant conversion was detected below 80 ℃. The best temperature that gave clearly discernible ¹H NMR signals for HMF (**3**) was from 80-100 ℃. When held at this temperature then increasing time shows a corresponding increase in signals for HMF (see Figure S7 A&B of ESI). Thus, armed with this knowledge the dehydration reaction was further investigated at 100 ℃.

### In an atmosphere of air (¹H and ¹³C NMR study)

The results and discussion introduced in this section represent the dehydration of D-fructose (**2**) (180 mg, 1mmol) catalysed by Fe-NHC (**1a**) (38 mg, 0.01 mmol) Fe-NHC (**1b**) (32 mg, 0.01

mmol) at 100 °C in DMSO-$d_6$ (4 mL) for 10 min, 20 min, 30 min, 1 h, 3 h and 6 h in an air atmosphere. The progress of the dehydration reaction was monitored by nmr spectroscopy ($^1$H and $^{13}$C) both *insitu* and batch. Figure S7 A of ESI, shows the stacked $^1$H NMR spectra at 100 °C for the dehydration of fructose (**2**) in the presence of Fe-NHC catalyst (**1**) supported on expanded HACS and Starbon™ 350 respectively at t= 10 min, 20 min, 0.5 h, 1 h, 3 h and 6 h. At a purely qualitative level the dehydration of fructose (**2**) is characterized by a darkening of the reaction colour from clear pale yellow (0.5 h) to light brown (1 h to 3 h) to dark brown (6 h) over time. The onset of the dark brown colour is characteristic of HMF decomposition to levulinic acid and humins (see later) as discussed earlier. [34,35]

$^1$H NMR (DMSO-$d_6$ ,400MHz): □ = 9.49 (s, 1 H), 7.44 (d, *J*=3.2 Hz, 1 H), 6.55 (d, *J*=3.2 Hz, 1 H), 4.46 ppm (s, 2 H)

The signal at 2.45 ppm is assigned to DMSO- $d_6$, [36] whilst complex multiplets for fructose are in the region 3-5 ppm. [37] As can be seen from figure S7 A of ESI, corresponding to fructose conversion using the Fe-NHC expanded HACS (**1a**), weak signals at 7.44 ppm, 6.55 ppm and 4.46 ppm starts to appear at 10 min reaction time which develop in intensity as the reaction proceeds over time. HMF (3) is clearly evident at 30 min ((1 H, **H**-C=O, 9.49 ppm), (1H, O=C-C=C**H**, 7.44 ppm), (1H, H$_2$C-C=C**H**-, 6.55 ppm) and (2H, HO-C**H$_2$** -C=CH, 4.46 ppm)) coupled with significant reduction in the signals for fructose. The signal at 8.08 ppm was assigned to formic acid which is formed due to the addition of two water molecules as a consequence of the reverse hydrolysis reaction that is considered as one of the side reactions of fructose conversion to HMF. [38 39] Interestingly, the intensity of HMF signals starts to declined slightly after 1 h reaction time which may be due to the re-hydration side reaction to formic acid and levulinic acid. This observation is confirmed by HPLC results given later in which the HMF yield calculated after 1 h reaction time is less than that at t = 1 h.

However, in figure S7 B of ESI corresponding to fructose conversion with Fe-NHC Starbon™ 350 (**1b**), HMF signals were evident at t= 20 min, coupled with almost the disappearance of the signals from fructose at 3.3-4.3 ppm. Interestingly, the intensity of HMF signals also declined after 1 h reaction time which may be due to the re-hydration side reactions.

The complementary $^{13}$C NMR investigation (see Figure S8 A&B of ESI) also revealed a decrease in signals of fructose coupled with an increase in signals for HMF with respect to time. The signals for DMSO-d6 are present at 39.5 ppm whilst those for fructose are in the range 60 - 105 ppm. In figure 14, HMF signals were evident at t=0.5 h (56.43 ppm, HO-C**H$_2$**-C=CH-), (110.24 ppm, HO-CH$_2$-C=C**H**-), (152.25 ppm, O=HC-C**H**=C-), (162.66 ppm, HO-CH$_2$-**C**=CH$_2$-) and 178.53 ppm, O=**C**H-C=CH)). [40] Signals at 31.19 ppm and 204.9 ppm are attributed to a carbonyl containing species yet to be fully determined. The signal at 163.45 ppm most likely corresponds to formic acid which agrees with its $^1$H NMR peak observed.

In our situation, conversion occurs at 80-100 °C in the presence of Fe-NHC catalyst (**1**). Based on the work of J. Guan et al, [40] we propose the following mechanism (Figure 13) for conversion of fructose (**2**) to HMF (**3**). The iron (Fe$^{3+}$) coordinates with the carbonyl and adjacent OH within fructose to form a metal fructofuranose complex. A series of three dehydrations (-3 H$_2$O) induced by the catalyst attaching and detaching the fructose ring structure affords the desired HMF (**3**).
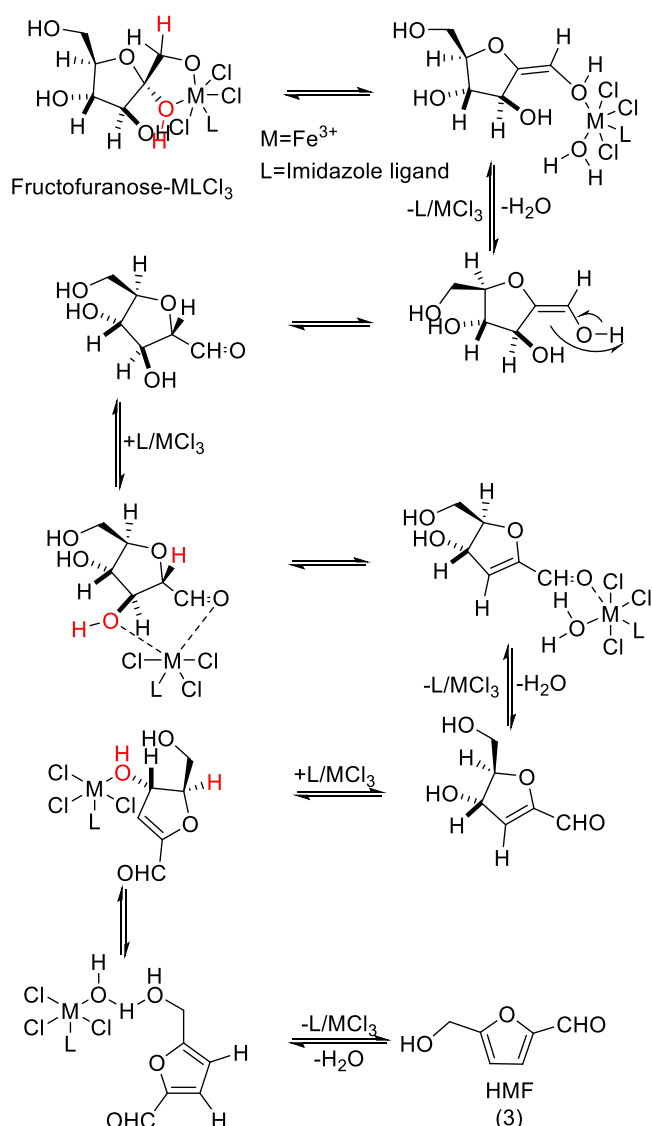


Figure 13. Proposed mechanism for fructose dehydration to HMF with Fe-NHC catalyst (**1a-b**)

## Quantification via HPLC

The progress of the reaction was also monitored by HPLC in order to better investigate yield and selectivity. The results are represented graphically in Figure 16. In figure 16A corresponding to conversion with Fe-NHC expanded HACS catalyst (1a), at 0.5-1 h, high HMF yield and selectivity (99 %) was obtained thus indicating effectiveness of our novel Fe-NHC (1) as a catalyst for fructose (2) dehydration to HMF (3). The high selectivity at this time could be explained by the low probability of re-hydration at this point compared to proceeding times. The best HMF yield with respect to time 86 %, TOF=206 h$^{-1}$ was obtained at t= 0.5 h. Thereafter, although fructose conversion is the highest (97 %) for 6 h reaction time both HMF yield and selectivity drop significantly. As proposed earlier this may be due to re-hydration to formic acid at 4.74 min retention time which is supported by the NMR analysis discussed before. Some other side products are recorded at different retention times. Among them, 3-furoic acid is identified at 7.88 min with 4.24% area.
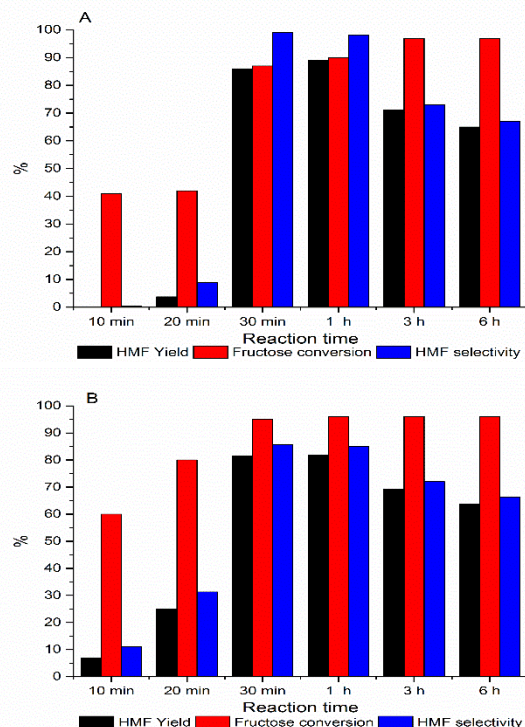
Figure 14. Fructose conversion, HMF yields and selectivity over Fe-NHC expanded HACS (**1a**, Top A) and Fe-NHC Starbon 350 (**1b**, Bottom B) catalysts. Conditions: D-fructose (180 mg, 1mmol), Fe-NHC (**1**) (32 mg, 0.01 mmol) at 100 °C in DMSO-$d_6$ (4 mL).

Figure 14B on the other hand, which corresponds to the catalytic conversion using the Fe-NHC Starbon™ 350 catalyst (**1b**), the best catalytic activity with HMF yield of 81.5 % (TOF=169 h$^{-1}$), fructose conversion of 95 % and HMF selectivity of 85.7 % at t=0.5 h. No significant changes occur on taking the reaction further to t=1 h. Thereafter, at t=3 h and t=6 h, both HMF yield and selectivity drops. As earlier stated, may be due to rehydration side reaction

**Catalyst recycling and reuse**

Catalyst recycling and re-use was investigated in DMSO-$d_6$ at 100 °C with each experiment being monitored by NMR (qualitative) and HPLC (quantitative). Conditions: D-fructose (180 mg, 1mmol), Fe-NHC (**1a**) (38 mg, 0.01 mmol), Fe-NHC (**1b**) (32 mg, 0.01 mmol) at 100 °C in DMSO-$d_6$ (4 mL), time 1 h. As shown by the quantitative data, Figure 15A below shows that, the desired Fe-NHC expanded HACS catalyst (**1a**) can be re-used up to four times (4x) without significant loss in performance; HPLC results reported 73.77%, 66.82%, 71.85%, 72.37% and 46.76% HMF yields with lowest fructose conversion of 88.03% for the second run and lowest selectivity of 52.81% for the last cycle. The NMR spectra reported show the existence of HMF signals in all 5 cycles of use. Hot filtration and ICP analysis of the leachate shows no discernible amounts of Fe (79.49 ppb), thus showing the integrity of our catalytic system.

Figure 15B corresponding to Fe-NHC Starbon™ 350 catalyst (**1b**) shows that the catalyst can also be re-used for up to five times without any significant loss in catalytic activity. HPLC results reported 83 %, 82 %, 83%, 81%, and 81% HMF yields over 5 cycles.
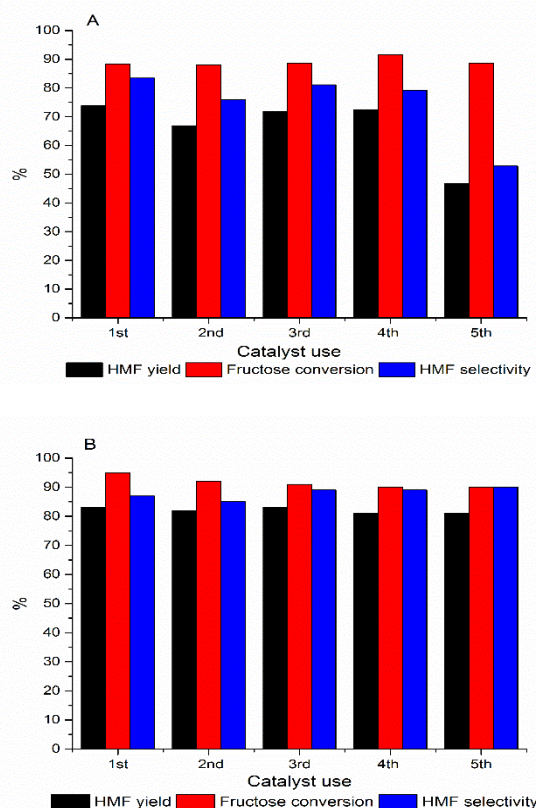


Figure 15. Reusability data for Fructose conversions, HMF yields and selectivities over Fe-NHC expanded HACS (**1a**, Top A) and Fe-NHC Starbon 350 (**1b**, Bottom B). Conditions: D-fructose (180 mg, 1mmol), Fe-NHC (**1a**) (38 mg, 0.01 mmol) Fe-NHC (**1b**) (32 mg, 0.01 mmol) at 100 °C in DMSO-d6 (4 mL), time 1 h.

**Fe-NHC catalyst (1) comparison with other heterogeneous catalysts (Amberlyst-15, Montmorillonite K-10 and ZSM-5 (Si:Al = 30)**

The acid-catalysed dehydration of fructose (**2**) to HMF (**3**) has been well investigated using a variety of heterogeneous catalysts, namely: Amberlyst-15, Montmorillonite K10 and ZSM-5 ($SiO_2$:$Al_2O_3$=30). Thus, to compare activity between these catalysts and our catalyst (**1**), a series of standard reactions were undertaken using the same amount of fructose and DMSO at 100 °C with the appropriate catalyst. Literature data was not used because lack of knowledge of exactly how the study was performed would add huge uncertainty when trying to compare data. Our methodology removes variables and introduces consistency of approach. Conditions: D-fructose (180 mg, 1mmol), catalyst loading (32 mg) at 100 °C in DMSO-$d_6$ (4 mL). The comparison was based on equal amount by weight of the catalysts employed. HPLC results for the comparative study are shown in Figure 16. Over Amberlyst-15, HMF yield occur at t=1 h and thereafter no significant increase in yield up to t=6 h. The behavior of Montmorillonite K-10 is almost a linear increment but with a bit of abnormality at t=1 h at which the yield and selectivity seemed to drop a little before a progressive increase with time up to t=6 h. ZSM-5 catalyst attains a good yield at t=6 h but no significant yield up to t=3 h. Expanded HACS supported Fe-NHC catalyst (**1a**) had its highest HMF yield at t= 1 h. However, for S350 Fe-NHC catalyst (**1b**) the fructose conversion, HMF yield and HMF selectivity, starts very high at initial reaction time of t=20 min to 1 h and thereafter the HMF yield start to drop significantly with increasing reaction time.
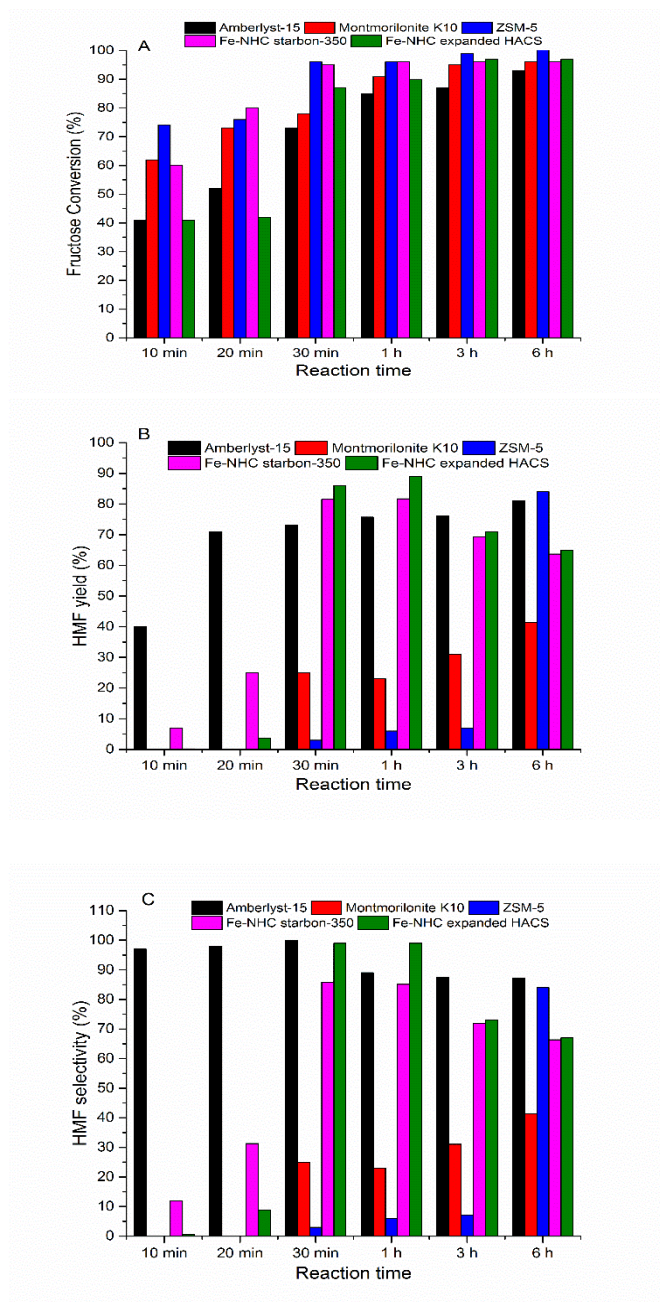
Figure 16. Comparative study of the fructose to HMF conversion (A), HMF Yield (B) and selectivity (C) with other catalysts.

Conditions: D-fructose (180 mg, 1 mmol), each catalyst (32 mg) at 100 ◦C in DMSO-d6 (4 mL).

## TEMPERATURE AND REACTION TIME STUDY ON THE FRUCTOSE TO HMF CONVERSION WITH Fe-NHC S350.

Figure 17 shows the influence of reaction temperature and time on the fructose conversion, HMF yield and HMF selectivity respectively, using the fabricated Fe-NHC Starbon™ 350 (**1b**) as reaction catalyst. Conditions: D-fructose (180 mg, 1mmol), Fe-NHC (**1**) (32 mg, 0.01 mmol) at 80 ℃ & 100 ℃ in DMSO-$d_6$ (4 mL). It can be inferred from the results above that increasing the reaction temperature from 80 to 100 ºC is very much beneficial if not crucial to achieving higher conversion, yield and selectivity of 96 %, 82 % and 85 % respectively, within shorter reaction time of 0.5-1 h as compared to fructose conversion, HMF yield and HMF selectivity of 53 %, 10 %, and 17 % respectively at reaction time 0.5-1 h, when explored at a lower reaction temperature of 80 ºC. At a lower reaction temperature of 80 ºC, longer reaction

time of 3 h is necessary to achieve good HMF yield of 75 %, as compared to 82 % HMF yield within just 0.5 h when explored at 100 ºC.
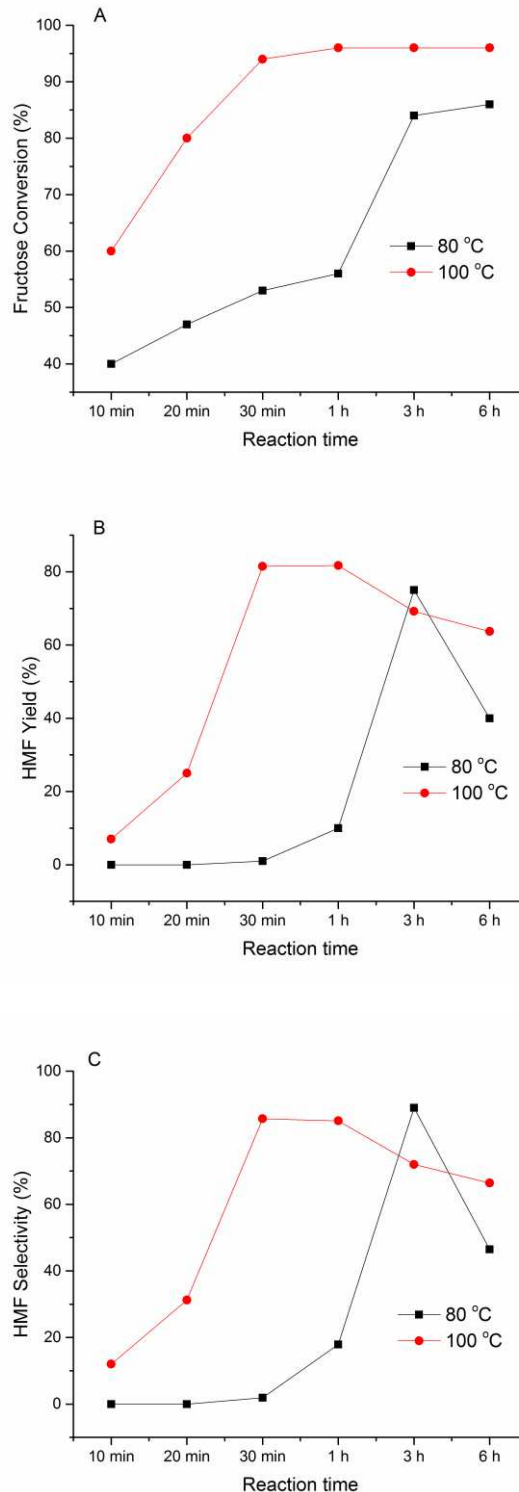


Figure 17. Fructose conversion (A), HMF yield (B) and HMF selectivity (C) at 80 ºC and 100 ºC for Starbon 350 catalyst (**1b**)

Taking reaction time into consideration, figure 17 indicates that at 100 ºC, prolonging the reaction after 1 h do not result in any

beneficial effect but results in decrease in HMF yield and selectivity. At 80 °C reaction temperature however, good fructose conversion, HMF yield and HMF selectivity were only achieved after a longer reaction time of 3 h. Prolonging the reaction from 3 h also resulted in decreasing yield and selectivity.
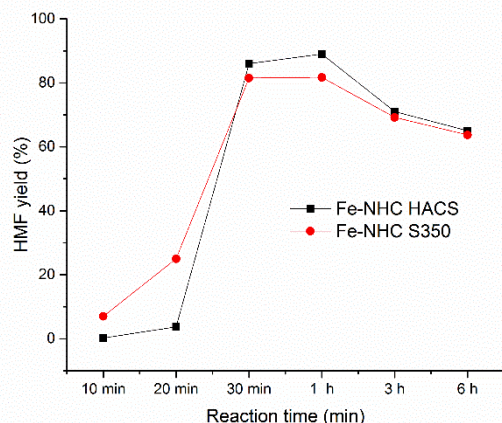


Figure 18. Reaction kinetic curve (yield vs time) for Fe-NHC HACS and Fe-NHC-Starbon™-350.

The kinetic profile (figure 18) based on HMF yield efficiency for two different supports employed, showed a similar HMF yield with slightly higher yield obtained with the Starbon-350 support at initial reaction time of 20 minutes. Highest yield was obtained with the HACS support at a later reaction time of 1 h. Both the two supports show a similar profile with yields falling after 1 h reaction time.

## Conclusions

The proposed HACS supported Fe-NHC catalyst (**1a**) and S350 supported Fe-NHC catalyst (**1b**) were fabricated successfully as confirmed by the various characterization techniques employed. Both mesoporous supports were effective for the immobilization of the Fe-NHC due to enhanced mesoporosity which offered functional space and overcome diffusion limitation for bulky reactants or products. The performance of the catalysts for heterogeneous catalytic conversion of fructose to HMF was investigated. A good yield of HMF (86 %) was achieved at 100 °C over 0.5 h reaction time using the expanded HACS immobilised Fe-NHC catalyst. However, the S350 immobilised Fe-NHC also gives HMF yield of (81.7 %) at reaction time of 0.5 h. Further work should be focused on optimization of the reaction conditions and catalyst/substrate loading to achieve higher HMF conversions and selectivity over even shorter reaction time. This however, is part of our future work.

## Experimental Section

The synthesis of Fe-NHC (**1a-b**) using a convergent strategy, from either expanded high amylose corn starch (HACS) (**4a**) or Starbon-350 (**4b**) and *N*-(3-aminopropyl) imidazole (**7**), is depicted in Figure 1. Starbon 350 was prepared in-house according to literature methods, where '350' signifies carbonisation temperature. All intermediates and final products were characterized by a variety of techniques. Instrument details, parameters and experimental procedures are detailed in ESI.

## Acknowledgements

## Associated content

The experimental section, proposed fructose dehydration mechanism, and XPS deconvolution data can be obtained from the ESI (electronic supplementary information).

### Corresponding Author

* Email. Avtar.matharu@york.ac.uk

### Author Contributions

The manuscript was written through contributions of all authors.

### Notes

The authors declare no competing financial interests.

## Abbreviations

HACS, high amylose corn starch; S350, Starbon 350; NHC, N-heterocyclic carbene; HMF, 5-(hydroxymethyl) furfural; IL, imidazolium ligand; DSC, disuccinimidyl carbonate; TFA, triflouro acetic acid; CPME, cyclopentyl methyl ether; TEA, triethylamine; TOF, turnover frequency.

## Acknowledgements

## References

[1] R. Zhong, A.C. Lindhorst, F.J. Groche, F.E. Kühn, *Chem Rev*. **2017**;117(3):1970-2058. doi:10.1021/acs.chemrev.6b00631.

[2] Y. Liu, P. Persson, V. Sundström, K. Wärnmark, *Acc Chem Res*. **2016**;49(8):1477-1485. doi:10.1021/acs.accounts.6b00186.

[3] D. S. Adhikary, D. Bose, P. Mitra, K. D. Saha, V. Bertolasi, J.Dinda, *New J Chem*. **2012**;36(3):759. doi:10.1039/c2nj20928d.

[4] J. I. Bates, D. P. Gates, *Organometallics*. **2012**;31(12):4529-4536. doi:10.1021/om3003174.

[5] R. Luque, M. J. Garcia, *ChemCatChem*. **2013**;5(4):827-829. doi:10.1002/cctc.201300110.

[6] I. Jiménez-Morales, M. Moreno-Recio, J. Santamaría-González, P. Maireles-Torres, A. Jiménez-López, *Appl Catal B Environ*. **2015**;164:70-76. doi:10.1016/j.apcatb.2014.09.002.

[7] H. Jin, M.B. Ansari, S. E. Park, *Catal Today*. **2014**;245:116-121. doi:10.1016/j.cattod.2014.05.021.

[8] R. J. White, R. Luque, V. L. Budarin, J. H. Clark, D. J. Macquarrie, *Chem Soc Rev*. **2009**;38(2):481-494. doi:10.1039/b802654h.

[9] E. Lam, J. H. T. Luong, *ACS Catal*. **2014**;4:3393-3410.

[10] V. L. Budarin, J. H. Clark, J. J. Hardy, *et al*. *Angew. Chem. Int. Ed. Engl*. **2006**;3782-3786. doi:10.1002/anie.200600460.

[11] R. J. White, V. L. Budarin, R. Luque, J. H. Clark, D. J. Macquarrie, *Chem Soc Rev*. **2009**;38(12):3401-3418. doi:10.1039/b822668g.

[12] Y. N. Li, J. Q. Wang, L. N. He, *et al.*, *Green Chem*. **2012**;14(10):2752. doi:10.1039/c2gc35845j.

[13] M. J. Climent, A. Corma, S. Iborra, *Green Chem*. **2014**;16(2):516. doi:10.1039/c3gc41492b.

[14] A. A. Rosatella, S. P. Simeonov, R. M. Frade, C. M. Afonso, *Green Chem*. **2011**;13(4):754. doi:10.1039/c0gc00401d.

[15] F. Delbecq, Y. Wang, C. Len, *Mol Catal*. **2017**;434:80-85. doi:10.1016/j.mcat.2017.02.037.

[16] K. Peng, X. Li, X. Liu, Y. Wang, *Mol Catal*. **2017**;441:72-80. doi:10.1016/j.mcat.2017.04.034.

[17] D. Garcés, E. Díaz, S. Ordóñez, *Ind Eng Chem Res*. **2017**;56(18):5221-5230. doi:10.1021/acs.iecr.7b00952.

[18] C. Schuh, J. Rühe, *Macromolecules*. **2011**;44(9):3502-3510. doi:10.1021/ma102410z.

[19] F. J. Warren, M. J. Gidley, B. M. Flanagan, *Carbohydr Polym*. **2016**;139:35-42. doi:10.1016/j.carbpol.2015.11.066.

[20] R. Kizil, J. Irudayaraj, K. Seetharaman, *J Agric Food Chem*. **2002**;50(14):3912-3918. doi:10.1021/jf011652p.

[21] I. Tan, B. M. Flanagan, P. J. Halley, A. K. Whittaker, M. J.Gidley, *Biomacromolecules*. **2007**;8(3):885-891. doi:10.1021/bm060988a.

[22] H. Tang, B. P. Hills, *Am Chem Soc*. **2003**;4(5):1269-1276.

[23] L. A. Sofia, A. Krishnan, M. Sankar, et al., *J Phys Chem C*. **2009**;113(50):21114-21122. doi:10.1021/jp906108e.

[24] J. D. Mao, K. Schmidt-Rohr, *Solid State Nucl Magn Reson*. **2004**;26(1):36-45. doi:10.1016/j.ssnmr.2003.09.003.

[25] J. Kaal, S. Brodowski, J. A. Baldock, K. J. Nierop, A. M. Cortizas, *Org Geochem*. **2008**;39(10):1415-1426. doi:10.1016/j.orggeochem.2008.06.011.

[26] B. S. Kaith, R. Jindal, A. K. Jana, M. Maiti, *Bioresour Technol*. **2010**;101(17):6843-6851. doi:10.1016/j.biortech.2010.03.113.

[27] A. Mishra, R. Sharma, B. D. Shrivastava, *Indian Journal of Pure & Applied Physics* **2011**;49(November):740-747.

[28] G. F. Moreira, E. R. Peçanha, M. M. Monte, S. L. Filho, F. Stavale, *Miner Eng*. **2017**;110(April):96-103. doi:10.1016/j.mineng.2017.04.014.

[29] J. H. Zhou, Z. J. Sui, J. Zhu, et al., *Carbon N Y*. **2007**;45(4):785-796. doi:10.1016/j.carbon.2006.11.019.

[30] J. Gurgul, K. ŁąTka, I. Hnat, J. Rynkowski, S. Dzwigaj, *Microporous Mesoporous Mater*. **2013**;168(MARCH):1-6. doi:10.1016/j.micromeso.2012.09.015.

[31] Z. Yan, Z. Zhuxia, L. Tianbao, L. Xuguang, X. Bingshe, *Spectrochim Acta - Part A Mol Biomol Spectrosc*. **2008**;70(5):1060-1064. doi:10.1016/j.saa.2007.10.031.

[32] A. P. Grosvenor, B. A. Kobe, M. C. Biesinger, N. S. McIntyre, *Surf Interface Anal*. **2004**;36(12):1564-1574. doi:10.1002/sia.1984.

[33] S. Diamanti, S. Arifuzzaman, A. Elsen, J. Genzer, R. Vaia, *Polymer (Guildf)*. **2008**;49(17):3770-3779. doi:10.1016/j.polymer.2008.06.020.

[34] C. Antonetti, D. Licursi, S. Fulignati, G. Valentini, A. Raspolli Galletti, *Catalysts*. **2016**;6(12):196. doi:10.3390/catal6120196.

[35] X. Qi, M. Watanabe, T. M. Aida, R. L. Smith, *Green Chem*. **2008**;10:799-805.

[36] H. E. Gottlieb, V. Kotlyar, A. Nudelman, *J Org Chem*. **1997**;62(21):7512-7515. doi:10.1021/jo971176v.

[37] B. Thomas, M. Ginic-Markovic, R. M. Johnston, P. Cooper, N. Petrovsky, *Carbohydr Res*. **2012**;347(1):136-141. doi:10.1021/nl061786n.Core-Shell.

[38] N. R. Babij, E. O. McCusker, G. T. Whiteker, et al., *Org Process Res Dev*. **2016**;20(3):661-667. doi:10.1021/acs.oprd.5b00417.

[39] E. L. S. Ngee, Y. Gao, X. Chen, et al., *Ind Eng Chem Res*. **2014**;53(37):14225-14233. doi:10.1021/ie501980t.

[40] J. Guan, Q. Cao, X. Guo, X. Mu, *Comput Theor Chem*. **2011**;963(2-3):453-462. doi:10.1016/j.comptc.2010.11.012.

# Entry for the Table of Contents

## FULL PAPER
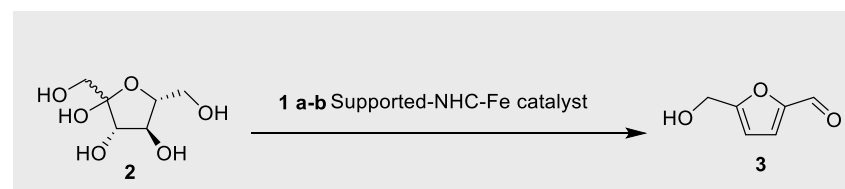
*[a]Avtar S. Matharu, [a]Duncan J. Macquarrie, [a]Suleiman Ahmed, [a]Badriya Al-monthery, [b]Yoon-Sik Lee and [b]Yohan Kim. Corresponding Author: *[a]Avtar S. Matharu*

*Page No.1 – Page No.12*

**Title: Novel Starbon/HACS-supported *N*-heterocyclic carbene-iron(III) catalyst for efficient conversion of fructose to HMF.**

Text for Table of Contents: Abstract, Introduction, Results and discussion, Conclusions, Experimental, Acknowledgement, Associated content, Abbreviations, References.

# Captions for figures:

Figure 1. Synthetic route to iron-NHC catalysts 1a and 1b.

Figure 5. FT-IR spectra for expanded HACS (4a), succinimidyl carbonate activated HACS (6a), ligand grafted DSC activated HACS (13a) and Fe-NHC catalyst (1a).

Figure 6.FT-IR spectra for S350 (**4b**), succinimidyl carbonate activated S350 (**6b**), ligand grafted S350 (**13b**) and Fe-NHC S350 (catalyst) (**1b**).

Figure 7.. $^{13}$C CPMAS NMR spectra for expanded HACS (**4a**), succinimidyl carbonate activated HACS (**6a**), ligand grafted activated HACS (**13a**) and Fe-NHC catalyst (**1a**)

Figure 8.$^{13}$C CPMAS NMR spectra for Starbon 350 (**4b**), succinimidyl carbonate activated S350 (**6b**), ligand grafted activated S350 (**13b**) and Fe-NHC catalyst (**1b**)

Figure 6.  TG (top) and dTG (bottom) for expanded HACS (**4a**), succinimidyl carbonate activated HACS (**6a**), ligand grafted DSC activated HACS (**13a**) and Fe-NHC catalyst (**1a**).

Figure 7.  TG (top) and DTG (bottom) for Starbon 350 (**4b**), succinimidyl carbonate activated Starbon 350 (**6b**), ligand grafted Starbon 350 (**13b**) and Starbon 350 Fe-NHC catalyst (**1b**).

Figure 8. Mössbauer spectrum of Fe-NHC expanded HACS (Top, **1a**) and Fe-NHC Starbon 350 (Bottom, **1b**).

Figure 9. XPS survey data of (A) Expanded HACS (**4a**) (B) Starbon 350 (**4b**).

Figure 10. XPS survey data of (A) Fe-NHC HACS catalyst (**1a**) (B) Fe-NHC starbon 350 catalyst (**1b**).

Figure 11.  SEM micrographs of (A) expanded HACS (**4a**) (B) Ligand grafted expanded HACS (**13a**) and (C) Fe-NHC expanded HACS (**1a**).

Figure 12.  SEM micrographs of (1) Starbon 350 (**4b**), (2) Ligand grafted Starbon 350 (**13b**) and (3) Fe-NHC Starbon 350 (**1b**).

Figure 13. Proposed mechanism for fructose dehydration to HMF with Fe-NHC catalyst (**1a-b**)

Figure 14. Fructose conversion, HMF yields and selectivity over Fe-NHC expanded HACS (**1a**, Top A) and Fe-NHC Starbon 350 (**1b**, Bottom B) catalysts. Conditions: D-fructose (180 mg, 1mmol), Fe-NHC (**1**) (32 mg, 0.01 mmol) at 100 ℃ in DMSO-$d_6$ (4 mL).

Figure 15.  Reusability data for Fructose conversions, HMF yields and selectivities over Fe-NHC expanded HACS (**1a**, Top A) and Fe-NHC Starbon 350 (**1b**, Bottom B). Conditions: D-fructose (180 mg, 1mmol), Fe-NHC (**1a**) (38 mg, 0.01 mmol) Fe-NHC (1**b**) (32 mg, 0.01 mmol) at 100 ∘C in DMSO-d6 (4 mL), time 1 h.

Figure 16. Comparative study of the fructose to HMF conversion (A), HMF Yield (B) and selectivity (C) with other catalysts.
Conditions: D-fructose (180 mg, 1 mmol), each catalyst (32 mg) at 100 ∘C in DMSO-d6 (4 mL).

Figure 17. Fructose conversion (A), HMF yield (B) and HMF selectivity (C) at 80 ℃ and 100 ℃ for Starbon 350 catalyst (**1b**)

Figure 18. Reaction kinetic curve (yield vs time) for Fe-NHC HACS and Fe-NHC-Starbon$^{TM}$-350.